DOI: https://doi.org/10.2138/am-2021-7726. http://www.minsocam.org/

Word count: 7481

Revision 1

Heat Capacity and Thermodynamic Functions of Partially Dehydrated Sodium and Zinc Zeolite A (LTA)

Matthew S. Dickson[1], Peter F. Rosen[1], Grace Neilsen[1], Jason J. Calvin[1], Alexandra Navrotsky[2], and Brian F. Woodfield*[1]

[1]Department of Chemistry and Biochemistry, Brigham Young University, Provo, UT 84602, U.S.A.

[2]School of Molecular Sciences and Center for Materials of the Universe, Arizona State University, Tempe, Arizona 85281, U.S.A.

*Corresponding author. Tel.: +1 801 422 2093; fax: +1 801 422 0153
Email address: brian_woodfield@byu.edu (B. F. Woodfield)

Abstract

Zeolite A (LTA) is an industrially important zeolite that exhibits sorption-induced framework flexibility, the thermodynamics of which are poorly understood. In this work, we report heat capacity measurements on zinc and sodium zeolite A from 1.8 K to 300 K and compare the heat capacity of water in sodium zeolite A with that of water in other zeolites. The heat capacity of zeolitic water varies significantly depending on hydration level and identity of the host zeolite, and more tightly bound water exhibits strong inflections in its heat capacity curve. This suggests a combination of effects, including differences in water-framework binding strength and hydration-dependent flexibility transitions. We also report fits of the heat capacity data using theoretical functions, and values for $C_{p,m}°$, $\Delta_0^{\mathrm{T}}S_{\mathrm{m}}°$, $\Delta_0^{\mathrm{T}}H_{\mathrm{m}}°$, and $\Phi_{\mathrm{m}}°$ from 0 K to 300 K. These results contribute to a systematic thermodynamic understanding of the effects of cation exchange, guest molecule confinement, and sorbate-dependent flexibility transitions in zeolites.

KEYWORDS: Zeolite, framework flexibility, gate opening, zeolitic water, heat capacity

Introduction

Zeolite A (also known as Linde-Type A or LTA) is a microporous aluminosilicate material that has found wide application in industry for selective sorption (Auerbach et al., 2003; Kim et al., 2016; Yin et al., 2005), molecular sieving (Auerbach et al., 2003; Yin et al., 2005), ion exchange(Auerbach et al., 2003), gas separation (Auerbach et al., 2003; Kim et al., 2016; Yin et al., 2005), and catalysis (Auerbach et al., 2003; Chen, 1996; Öhlmann et al., 1991). The many uses of zeolite A, like those of other porous crystalline frameworks (e.g. metal-organic frameworks), are based on interactions between the framework itself and guest molecules introduced into its structure. There is evidence that some porous crystalline frameworks, including zeolite A, exhibit novel behaviors such as framework flexibility and the related phenomenon gate opening (Guo and Navrotsky, 2018; Guo et al., 2018). Both phenomena involve structural changes that are induced by guest molecules and alter the material's sorptive properties. Understanding the thermodynamics of such sorption-based phenomena is necessary to design useful new framework materials.

Zeolite A is composed of a framework of alternating corner-sharing SiO_4 and AlO_4 tetrahedra, which form a cubic structure of eight alpha cages (supercages) and eight beta cages (sodalite) (Loewenstein, 1954). Extra-framework cations (typically Na^+) located in the cages of the structure balance the net negative charge caused by substitution of Al^{3+} for Si^{4+}. By exchanging different cations into the structure, it is possible to modify the pore properties, structural properties, and catalytic activity of a zeolite (Armor, 1998; Guo et al., 2018; Sun et al., 2016). Transition-metal-exchanged zeolites are of particular interest for properties such as variable oxidation states and multi-coordination capacity, and they exhibit exceptionally high catalytic activity for a number of useful redox reactions (Armor, 1998; Chatterjee et al., 1992).

This paper deals with several ion-exchanged versions of zeolite A, which we will refer to using abbreviations of the form M-A, where M is the extra-framework cation (e.g., Na-A and Zn-A).

Thermodynamic studies on porous frameworks both with and without guest molecules provide crucial information about the energetics of confinement. The present work is part of a collaborative investigation of the thermodynamics of strategically chosen synthetic zeolites with controlled variations in structure, cation content, and sorbate content (Guo and Navrotsky, 2018; Guo et al., 2019; Guo et al., 2018; Sun et al., 2016; Wu and Navrotsky, 2016; Yang and Navrotsky, 2000).

The Flexibility Transition in Zeolite A

In addition to their industrial importance, the zeolites in this study are of interest for exhibiting a “gate opening” or “flexibility” transition when partially dehydrated, as described by Guo and coworkers (Guo and Navrotsky, 2018; Guo et al., 2018). The presence of the transition defines three distinct hydration regimes: a low hydration phase (which exists from ~0–20% hydration), a transition or “two-phase” region (~20–50% hydration, or roughly 0.2–0.6 mol H_2O per $Al_xSi_yO_2$ tetrahedron), and a high-hydration phase (above ~50% hydration). (Note that “100 %” or “full” hydration is often defined somewhat arbitrarily as equilibrated with ambient conditions, and we use terms “fully hydrated” and “equilibrated with ambient” interchangeably.) The transition region is marked by a gradual structural change between low- and high-hydration phases, and the exact range over which it occurs depends on the identity of the extra-framework cation.

The flexibility transition has been studied in the greatest detail for sodium zeolite A (Na-A). Time-resolved XRD has shown a complex set of changes, including lattice contraction with increasing hydration prior to the transition followed by rapid expansion during the transition

(Guo and Navrotsky, 2018). Although these types of sorption-induced lattice changes can have important effects on zeolite performance, limited information on them is available.

Low-temperature Heat Capacity Measurements on Zeolites

The sensitivity of heat capacity data to changes in a material's density of states offers a unique perspective into sorption-induced flexibility transitions (Dickson et al., 2019; Rosen et al., 2020). Thus, heat capacity is a promising way to investigate the flexibility transition uncovered by Guo and coworkers (Guo and Navrotsky, 2018; Guo et al., 2018) in ion-exchanged zeolite A.

There are approximately 40 low-temperature heat capacity measurements on zeolites available in the literature (for a list see Voskov et al., 2019). All use the adiabatic method to measure heat capacity, and all deal with fully hydrated zeolites equilibrated with a variety of ambient humidities except for three studies (Johnson et al., 1982; Johnson et al., 1992; Qiu et al., 2000) that involve fully dehydrated zeolites. Four main problems are present in the literature that make it difficult to make meaningful comparisons between zeolites: (1) Characterization is sometimes incomplete (Haly, 1972; Qiu et al., 2006; Qiu et al., 2000). (2) All but three studies (Donahoe et al., 1990; Qiu et al., 2006; Qiu et al., 2000) focus on natural zeolites with widely varying compositions, which makes drawing conclusions about the relationship between structure and functional properties difficult (Qiu et al., 2000; Voskov et al., 2019). (3) Some works (Donahoe et al., 1990; Haly, 1972; Hemingway and Robie, 1984; Johnson et al., 1982; Johnson et al., 1983) do not clearly take precautions to prevent hydrated zeolites from losing water under vacuum while the sample is being mounted in the calorimeter. (For techniques that address this issue see Drebushchak, 1990; Johnson et al., 1985; and Paukov et al., 1997). Since water can comprise 60 % of a zeolite's heat capacity (Johnson et al., 1992), this renders the data inconsistent. (4) Other works (Hemingway and Robie, 1984; Johnson et al., 1983; Johnson et al., 1985; King, 1955) adjust measured heat capacities to predict the heat capacity of samples with an idealized composition or water content without adequately assessing whether these adjustments are appropriate. Such adjustments typically rely on analogies between zeolites and other minerals without accounting for special phenomena that zeolites can exhibit (Hemingway and Robie, 1984). In particular, the effect of hydration on zeolite heat capacity is unpredictable due to both possible flexibility transitions (Johnson et al., 1982; Vieillard, 2010) and variable water heat capacity that depends strongly on hydration level and zeolite identity (Hemingway and Robie, 1984; Neuhoff and Wang, 2007).

The low-temperature literature measurements with full characterization and known water content are plotted in Figure 1. Molecular formulas were adjusted to the form (Cations)$Al_xSi_yO_2$ and are given in Table 1. This comparison shows that the heat capacity (and therefore standard entropy and enthalpy) of zeolites varies widely. Thus, variations in structure, cation content, Si/Al ratio, and water content have major effects on zeolite energetics. However, the issue of variation in water content makes gaining insight from the comparison difficult. Since all available literature measurements deal with either fully hydrated or fully dehydrated specimens, it is difficult to separate the heat capacity effect of variable water surface interactions from that of flexibility transitions in the host zeolite. Thus, systematic heat capacity studies on zeolites to investigate these two aspects of water sorption are needed, particularly in the little-explored region of partial hydration.

This work is the first in a series reporting the results of heat capacity measurements on zeolites with a variety of hydration levels and no additional guest molecules. This effort will lay the groundwork for mapping the free energy landscape of several model zeolites and pave the way for future heat capacity studies on loaded zeolites. These papers will cover eight zeolites: five versions of zeolite A (unmodified Na-A and the exchanged versions Zn-A, Cu-A, Fe-A, and Mn-A) and three versions of the related zeolite RHO (unexchanged Na,Cs-RHO and the exchanged versions Cd,Cs-RHO and Li-H-RHO).

The present paper is concerned with Na-A and the ion-exchanged version Zn-A. Both are partially dehydrated, with Zn-A near the high-hydration end of the flexibility transition and Na-A near the low-hydration end. Heat capacities from 1.8 K to 300 K are reported, along with fits of the data and standard thermodynamic functions for each zeolite. The heat capacity of zeolitic water in Na-A is compared with that of water in other zeolites.

Experimental Methods

Sample Preparation

Synthetic zeolite A (NIST Standard Reference Material 8851) was used for the Na-A sample and as the starting material for Zn-A, which was prepared via an aqueous solution exchange (99.2% exchange) described elsewhere (Guo et al., 2018). Phase purity was confirmed by powder X-ray diffraction (XRD) and composition was determined via electron microprobe analysis (Guo et al., 2018; Sun et al., 2016). The samples have been explored previously using gas absorption calorimetry (Guo et al., 2018), time-resolved XRD (Guo and Navrotsky, 2018), differential scanning calorimetry (DSC) (Guo et al., 2018; Sun et al., 2016), and high temperature oxide melt drop solution calorimetry (Sun et al., 2016). Each sample was partially dehydrated in a vacuum oven (Na-A at 300 °C for 12 hours, Zn-A at 200 °C for 2 hours at approximately 6 kPa), and the remaining water content was determined by TGA analysis using a Mettler Toledo TGA/DSC 1 STARe System. TGA curves are provided in the Supplemental Material. Sample compositions, including water content, are listed in Table 2.

Both samples were dehydrated to within the two-phase region of the hydration-dependent flexibility transition. The Na-A sample (Na-A·0.23 H_2O) was near the low-hydration end of its transition, which takes place between 0.18 and 0.50 mol H_2O per mol zeolite (Guo and Navrotsky, 2018) and the Zn-A sample (Zn-A·0.58 H_2O) was near the high-hydration end of its transition, which takes place between 0.35 and 0.63 mol H_2O per mol (Guo et al., 2018).

Heat capacity measurements

The heat capacity of Na-A·0.23 H_2O and Zn-A·0.58 H_2O was measured from 1.8 K to 300 K on a Physical Property Measurement System (PPMS) from Quantum Design. Each sample was encased in copper foil (0.025 mm thick and 99.999% pure from Alfa Aesar) and compressed into a pellet in preparation for the measurement (Shi et al., 2011), with a coil of copper foil embedded in the pellet to improve thermal conductivity. The heat capacity of the sample holder and the Apiezon N grease thermally linking the sample to the holder were accounted for by a correction measurement performed prior to the sample measurement, and the heat capacity of the copper was subtracted from the measured heat capacity. Details on the sample pellets, including the mass of each material included in the measurement, are given in Table 3.

Because fully hydrated zeolites are known to lose water under vacuum above 260 K (Johnson et al., 1985; Paukov et al., 1997), we investigated the tendency of our partially dehydrated samples to lose water during the measurement. Na-A·0.23 H_2O was placed under vacuum at room temperature for three hours, which is the length of time the sample spends under vacuum above 260 K during the measurement. No change in the sample's mass was detected, so we conclude that the water content was stable during the measurement.

Results and Discussion

The measured heat capacities for Na-A·0.23 H_2O and Zn-A·0.58 H_2O are given in Tables 4 and 5 and a plot of the data (with literature data for the heat capacity of fully dehydrated Na-A from Qiu et al., 2000) is given in Figure 2. Note that there are likely small compositional differences between our sample of Na-A and the literature sample, which was assumed to have the ideal formula of $Na_{0.5}Si_{0.5}Al_{0.5}O_2$. The heat capacities are smooth and free of anomalies across the entire temperature range.

Heat Capacity of Zn-A vs Na-A

The heat capacity curves of Na-A·0.23 H_2O and Zn-A·0.58 H_2O are expected to have the same general form, with a (minor) difference in shape and (potentially large) difference in magnitude due to unequal numbers of cations and guest water molecules. Apparently, the increase in heat capacity from the extra water molecules in Zn-A is outweighed by the decrease in heat capacity caused by substitution of one Zn^{2+} for every two Na^+, resulting in an overall lower heat capacity in Zn-A. Another contributing factor is possibly stronger ion-framework (Wu and Navrotsky, 2016) and water-framework bonds (Guo et al., 2018) in Zn-A than in Na-A at the hydration levels investigated in this study. Stronger bonds increase the frequency of vibrational modes and cause them to turn on at higher temperatures, resulting in a lower heat capacity at a given temperature. Thus, the low heat capacity of Zn-A relative to Na-A reflects a combination of the effects of bond strength and the number of guest ions and molecules.

Heat Capacity of Zeolitic Water

The presence of water in Na-A·0.23 H_2O results in a heat capacity up to 16 % higher than the literature values for fully dehydrated Na-A. The lack of a broad water fusion anomaly above 260 K indicates that the water in the partially dehydrated sample is relatively tightly bound to the zeolite, with limited opportunity for bulk-like intermolecular interactions. It is important to note that the difference between the two data sets for Na-A, which we refer to as "apparent water heat capacity," reflects both the heat capacity of zeolitic water in Na-A and differences in framework heat capacity due to hydration-induced structural differences between the two samples. These changes include lattice contraction from 0 to 0.18 mol H_2O per mol Na-A, followed by a brief but more dramatic expansion from 0.18 to 0.23 mol H_2O (Guo and Navrotsky, 2018). In addition, any lattice changes that occur as a function of temperature would add to the heat capacity over the temperature range of their transition. The change in heat capacity attributable to both lattice changes and the water itself was calculated by taking the difference between fits of the two data sets, with the fit of the literature data consisting of one Debye and two Einstein functions. The result is plotted in Figure 3, where it is compared with similar apparent water heat capacities calculated from the literature.

Differences between the apparant water heat capacities for the five zeolites in Figure 3 demonstrate the upredictable behavior of zeolitic water. All five zeolitic water curves reflect the average behavior of sorbed water, calculated by taking the difference between two heat capacity curves for samples of the same zeolite with distinct hydration levels and dividing by the difference in moles of water. However, the curves in Figure 3 reflect the behavior of different "levels" of water in the zeolites because they were calculated from data on samples at different degrees of hydration. Thus, we refer to the water described in the curve for natrolite (which reflects the average behavior of the water between 0.42 and 0.62 mol H_2O per mol zeolite) as "loosely bound," and the water described by the curve for Na-A (0 vs 0.23 mol H_2O; full hydration is around 1 mol) as "tightly bound." The curves for analcime and mordenite reflect the average behavior for both loosely and tightly bound water because they were calculated from the difference between data for fully dehydrated samples and samples equilibrated with ambient conditions (0 vs 0.33 mol H_2O for analcime and 0 vs 0.58 mol H_2O for mordenite).

The apparent water heat capacity of laumontite is unique in that it describes "very loosely bound" water, reflecting the difference between ambient and above-ambient hydration (0.62 vs 0.72 mol H_2O). (Note that some authors refer to the ambient-hydration phase of laumontite using the historical term "leonhardite.") Anomalies similar to those at 210 K, 250 K, and above 300 K have been observed in a number of zeolite heat capacities (Basler and Lechert, 1972; Donahoe et al., 1990; Paukov et al., 1998b; Paukov et al., 2005), and are typically attributed to rearrangement in the water-cation subsystem, as they are in this case (Paukov and Fursenko, 1998a).

While comparisons between different zeolites have limitied *quantitative* validity, the data in Figure 3 are still useful for identifying *qualitative* trends about the behavior of water in zeolites. The heat capacity curves used to calculate apparent water heat capacity for analcime, mordenite, natrolite, and Na-A lack dramatic water/cation rearrangement peaks, and therefore show that there are significant differences even in the absence of major extra-framework rearrangements. Note that the curve representing loosely bound water (on natrolite) is the smoothest, while the curve representing tightly bound water (on Na-A) has the strongest inflections, and the curves representing an average of all water "levels" (on mordenite and analcime) have moderate inflections. This suggests that there may be trends in the heat capacity curves of a particular "level" of water across zeolites, with loosely bound water exhibiting a smooth heat capacity and tightly bound water exhibiting a more strongly inflecting heat capacity. The data for the loosely bound water in natrolite is quite similar in form to the heat capacity of the outer layers of water on titania nanoparticles (Calvin et al., 2019), which do not exhibit flexibility. This suggests that the first water molecules to desorb from a zeolite have little interaction with the zeolite framework itself, and it seems reasonable that this loosely bound water would behave similarly between zeolites. If this is true, then all four zeolites may have strongly inflecting heat capacity curves for their tightly bound water, with the strength of inflections being partially masked in analcime and mordenite because the loosely bound water is averaged into the data.

Inflections in the heat capacity of tightly bound zeolitic water have several possible causes. Water mobility can cause broad peaked contributions to zeolite heat capacities, but this seems unlikely for the tightly bound water in Na-A. Because the features of the Na-A apparent water heat capacity qualitatively match those in the analcime and mordenite data, it seems probable that they have a common source. A more promising possible explanation is framework flexibility, either due to structural differences between hydrated and dehydrated samples or possibly shifts in lattice parameters that become favorable at low temperatures and appear as a peaked contribution, like those observed in a metal-organic framework by Rosen et al., 2020.

The heat capacity of zeolitic water in Na-A is unique in that it is lower than the heat capacity of hexagonal ice for the majority of the measurement's temperature range. One potential cause of low heat capacity is strong bonding, which increases the frequency and energy of lattice vibrational modes and results in them turning on at higher temperatures. Thus, the low heat capacity of the zeolitic water in Na-A could reflect tighter binding of the low-level water with the strongly charged framework/cation system than either water-water hydrogen bonds or water-zeolite bonds in the other zeolites. This is likely aided by the strong charge of the zeolite A framework, which is the result of zeolite A having the lowest Si/Al ratio possible in a zeolite (equal to 1, as opposed to 2.1 for analcime or 3.1 for heulandite). The water in analcime and mordenite, on the other hand, has a higher heat capacity than that of hexagonal ice. This is surprising; since these data sets reflect an average of all water in the zeolite, we would expect the water heat capacity to lie between that of the tightly bound water in Na-A and the loosely bound water in natrolite. The high heat capacity may suggest that phenomena other than binding strength are at play, such as structural transformations.

While the contributions of unique water-zeolite interactions and framework flexibility are difficult to separate based on the information presently available, future work with different levels of hydration and different sorbates will enable comparisons that will enhance our understanding of zeolite sorption and framework flexibility.

Data Fitting and Thermodynamic Calculations

Fits of the measured heat capacity of Na-A·0.23 H_2O and Zn-A·0.58 H_2O were applied to low temperature (<15 K) and high temperature (>50 K) regions, and the two regions were connected using an orthogonal polynomial fit. Parameters for these fits are given in Table 6.

The heat capacities below 15 K were fit to the function

$$C_{low\,T} = \gamma T + B_3T^3 + B_5T^5 + B_7T^7 + B_{gap}T^ne^{-\frac{\delta}{T}}\#(1)$$

where γ, B_3, B_5, B_7, B_{gap}, n, and δ are adjustable parameters. B_3, B_5, and B_7 reflect the lattice heat capacity, with B_5 and B_7 correcting for anharmonicity in lattice vibrations. The remaining two terms were required to prevent systematic deviations from the fit. The need for the linear term γT, which would typically reflect the electronic heat capacity of a metal, can reflect lattice vacancies in insulators like zeolite A (Schliesser and Woodfield, 2015b). The final term models a Debye heat capacity contribution with a gap in the density of states. B_{gap} reflects the number of excess low-frequency modes with a gap, δ is proportional to the size of the gap, and n is the dimensionality of the vibrations. In this and other cases (Schliesser and Woodfield, 2015a) where

DOI: https://doi.org/10.2138/am-2021-7726. http://www.minsocam.org/

zeolite data were fit, $n = 1$ yielded the best results, which may reflect psudeo-linear vibrations that run along the wireframe-like structure of Na-A.

Above 50 K, the data were fit to the equation

$$C_{high\,T} = m \cdot D\left(\frac{\Theta_D}{T}\right) + n_1 \cdot E\left(\frac{\Theta_{E1}}{T}\right) + n_2 \cdot E\left(\frac{\Theta_{E2}}{T}\right) \#(2)$$

where $D(\Theta_D/T)$ and $E(\Theta_E/T)$ are Debye and Einstein functions, respectively, and m, n_1, n_2, Θ_D, Θ_{E1}, and Θ_{E2} are adjustable parameters (Gopal, 2012), with the latter three being characteristic Debye and Einstein temperatures. The Einstein contributions model two energies where the vibrational density of states is high, and the presence of the second Einstein contribution may reflect water or cation vibrations inside the pores.

The region from 10 K to 60 K was fit to an orthogonal polynomial according to the algorithm from Westrum's group (Justice, 1969), transformed into the form

$$C_{mid\,T} = \sum_{n=0,1,2\ldots 8} A_n T^n \#(3)$$

The fit in this temperature range is used to provide a smooth connection between the high and low temperature regions and is not physically meaningful.

The fits discussed above were used to calculate the standard molar thermodynamic functions $C_{p,m}°$, $\Delta_0^T S_m°$, $\Delta_0^T H_m°$, and $\Phi_m°$ from 0 K to 300 K. These functions are given in Tables 7 and 8. The standard molar entropies at 298.15 K are 76.3 and 66.3 J·K^{-1}·mol^{-1} for Na-A·0.23 H_2O and Zn-A·0.58 H_2O. Dividing by the number of atoms per formula unit yields an entropy per gram-atom (i.e., per mole of atoms) of 17.6 J·K^{-1}·g-atom^{-1} for Na-A and 13.3 J·K^{-1}·g-atom^{-1} for Zn-A. The higher entropy of Na-A suggests that the entropy contribution of its additional cations outweighs that of the extra water in Zn-A on a per-atom basis.

Implications

This study provides a thermodynamic perspective into the phenomena of cation exchange, water sorption, and sorbate-induced structural transformations in zeolites. Understanding these phenomena is key for implementing zeolites in their myriad applications, as well as for designing useful new zeolites. The presence of features common to the heat capacity of water in several zeolites, including sodium zeolite A (Na-A), suggests that the hydration-influenced framework flexibility that has been found in zeolite A may be present in other zeolites as well. If this proves correct, it is possible that heat capacity measurements will prove a useful tool for detecting such transformations and probing their thermodynamics. Furthermore, the comparison of zeolite samples that are identical except for cation content contributes to a growing understanding of the effects of cation exchange. Future work will further expand understanding of zeolites by involving different cation content and levels of hydration.

Acknowledgements

This work was financially supported by a grant from the U.S. Department of Energy under grant DE-SC0016446. Sample synthesis was supported by the U.S. Department of Energy, Office of Basic Energy Sciences, under grant DE-FG02-97ER14749.

References

Armor, J. (1998) Metal-exchanged zeolites as catalysts. Microporous and mesoporous materials, 22(1-3), 451-456.

Auerbach, S.M., Carrado, K.A., and Dutta, P.K. (2003) Handbook of zeolite science and technology. CRC press.

Basler, W., and Lechert, H. (1972) Molwärmemessungen an adsorbiertem Wasser im Zeolithen Linde 13 X. Zeitschrift für Physikalische Chemie, 78(3_4), 199-204.

Calvin, J.J., Rosen, P.F., Ross, N.L., Navrotsky, A., and Woodfield, B.F. (2019) Review of surface water interactions with metal oxide nanoparticles. Journal of Materials Research, 34(3), 416-427.

Chatterjee, S., Greene, H.L., and Park, Y.J. (1992) Comparison of modified transition metal-exchanged zeolite catalysts for oxidation of chlorinated hydrocarbons. Journal of Catalysis, 138(1), 179-194.

Chen, N.-Y. (1996) Shape selective catalysis in industrial applications. CRC press.

Dickson, M.S., Calvin, J.J., Rosen, P.F., and Woodfield, B.F. (2019) Low-temperature heat capacity measurements on insulating powders sealed under pressure. The Journal of Chemical Thermodynamics, 136, 170-179.

Donahoe, R.J., Hemingway, B.S., and Liou, J. (1990) Thermochemical data for merlinoite; 1, Low-temperature heat capacities, entropies, and enthalpies of formation at 298.15 K of six synthetic samples having various Si/Al and Na/(Na+ K) ratios. American Mineralogist, 75(1-2), 188-200.

Drebushchak, V. (1990) Calorimetric studies on dehydrated zeolites: natrolite, heulandite, chabazite, and mordenite. Geochemistry International, 5, 123-130.

Flubacher, P., Leadbetter, A., and Morrison, J. (1960) Heat capacity of ice at low temperatures. The Journal of Chemical Physics, 33(6), 1751-1755.

Giauque, W., and Stout, J. (1936) The Entropy of Water and the Third Law of Thermodynamics. The Heat Capacity of Ice from 15 to 273° K. Journal of the American Chemical Society, 58(7), 1144-1150.

Gopal, E. (2012) Specific heats at low temperatures. Springer Science & Business Media.

Guo, X., and Navrotsky, A. (2018) Hydration dynamics in zeolite A–An X-ray diffraction and infrared spectroscopic study. Microporous and Mesoporous Materials, 268, 197-201.

Guo, X., Wu, L., Corbin, D.R., and Navrotsky, A. (2019) Thermochemistry of formation of ion exchanged zeolite RHO. Microporous and Mesoporous Materials, 274, 373-378.

Guo, X., Wu, L., and Navrotsky, A. (2018) Thermodynamic evidence of flexibility in H 2 O and CO 2 absorption of transition metal ion exchanged zeolite LTA. Physical Chemistry Chemical Physics, 20(6), 3970-3978.

Haida, O., Matsuo, T., Suga, H., and Seki, S. (1974) Calorimetric study of the glassy state X. Enthalpy relaxation at the glass-transition temperature of hexagonal ice. The Journal of Chemical Thermodynamics, 6(9), 815-825.

Haly, A. (1972) Specific heat of a synthetic zeolite and the heat of fusion of its absorbed water. Journal of Physics and Chemistry of Solids, 33(1), 129-137.

Handa, Y., and Klug, D. (1988) Heat capacity and glass transition behavior of amorphous ice. The Journal of Physical Chemistry, 92(12), 3323-3325.

This is the peer-reviewed, final accepted version for American Mineralogist, published by the Mineralogical Society of America.
The published version is subject to change. Cite as Authors (Year) Title. American Mineralogist, in press.
DOI: https://doi.org/10.2138/am-2021-7726. http://www.minsocam.org/

Hemingway, B.S., and Robie, R.A. (1984) Thermodynamic properties of zeolites: low-temperature heat capacities and thermodynamic functions for phillipsite and clinoptilolite. Estimates of the thermochemical properties of zeolitic water at low temperature. American Mineralogist, 69(7-8), 692-700.

Howell, D., Johnson, G., Tasker, I., O'Hare, P., and Wise, W. (1990) Thermodynamic properties of the zeolite stilbite. Zeolites, 10(6), 525-531.

Johnson, G., Flotow, H., and O'hare, P. (1982) Thermodynamic studies of zeolites: analcime and dehydrated analcime. American Mineralogist, 67(7-8), 736-748.

Johnson, G., Flotow, H., O'Hare, P., and Wise, W. (1983) Thermodynamic studies of zeolites; natrolite, mesolite and scolecite. American Mineralogist, 68(11-12), 1134-1145.

Johnson, G., Flotow, H., O'Hare, P., and Wise, W.S. (1985) Thermodynamic studies of zeolites: heulandite. American Mineralogist, 70(9-10), 1065-1071.

Johnson, G., Tasker, I., Flotow, H., O'Hare, P., and Wise, W. (1992) Thermodynamic studies of mordenite, dehydrated mordenite, and gibbsite. American Mineralogist, 77(1-2), 85-93.

Justice, B.H. (1969) Thermal data fitting with orthogonal functions and combined table generation. The FITAB Program. AEC Cryogenics Project, University of Michigan, Ann Arbor, Michigan.

Kim, K.-M., Oh, H.-T., Lim, S.-J., Ho, K., Park, Y., and Lee, C.-H. (2016) Adsorption equilibria of water vapor on zeolite 3A, zeolite 13X, and dealuminated Y zeolite. Journal of Chemical & Engineering Data, 61(4), 1547-1554.

King, E. (1955) Low Temperature Heat Capacity and Entropy at 298.16° K. of Analcite. Journal of the American Chemical Society, 77(8), 2192-2193.

Loewenstein, W. (1954) The distribution of aluminum in the tetrahedra of silicates and aluminates. American Mineralogist: Journal of Earth and Planetary Materials, 39(1-2), 92-96.

Neuhoff, P.S., and Wang, J. (2007) Heat capacity of hydration in zeolites. American Mineralogist, 92(8-9), 1358-1367.

Öhlmann, G., Pfeifer, H., and Fricke, R. (1991) Catalysis and adsorption by zeolites. Elsevier.

Paukov, I., and Belitskii, I. (2000a) Heat capacity and thermodynamic functions of the natural zeolite ferrierite from 7 to 320 K. Geochemistry International, 38(1), 101-104.

-. (2000b) Thermodynamic properties of thomsonite within the temperature range of 5.8-309 K. Geochemistry International, 38(4), 405-407.

Paukov, I., Belitskii, I., and Berezovskii, G. (1998a) Low-temperature thermodynamic properties of a natural zeolite, epistilbite. Geochemistry international, 36(6), 565-567.

-. (1998b) Low-temperature thermodynamic properties of bikitaite. Geochemistry international, 36(10), 968-970.

Paukov, I., Belitsky, I., Fursenko, B., and Kovalskaya, Y.I. (1997) Thermodynamic properties of natural stellerite at low temperatures. Geokhimiya, 10, 1070-1072.

Paukov, I., Belitsky, I., and Kovalevskaya, Y.A. (2001a) Thermodynamic properties of the natural zeolite gmelinite at low temperatures. The Journal of Chemical Thermodynamics, 33(12), 1687-1696.

Paukov, I., and Fursenko, B. (1998a) Low-temperature heat capacity and thermodynamic functions of laumontite. Геохимия(12), 1301-1303.

-. (1998b) Low-temperature heat capacity and thermodynamic properties of leonhardite. Geochemistry international, 36(5), 471-473.

Paukov, I., Kovalevskaya, Y., and Belitskii, I. (1998c) Heat Capacity and Thermodynamic Properties of Natural Zeolite Erionite from 7 to 322 K. Geochemistry international, 36(7), 663-665.

Paukov, I., Kovalevskaya, Y.A., and Belitskii, I. (2001b) Thermodynamic properties of the natural zeolites. Low-temperature heat capacity of brewsterite. Geochemistry International, 39(4), 410-413.

Paukov, I., Kovalevskaya, Y.A., Belitskii, I., and Fursenko, B. (2002a) Thermodynamic properties of primary leonhardite within a temperature range of 6-309 K. Geochemistry International, 40(6), 621-624.

Paukov, I., Kovalevskaya, Y.A., Drebushchak, V., and Seretkin, Y.V. (2005) The thermodynamic properties of the thallium substituted natrolite form at low temperatures. Russian Journal of Physical Chemistry A, 79(12), 1926-1930.

Paukov, I., Moroz, N., Kovalevskaya, Y.A., and Belitsky, I. (2002b) Low-temperature thermodynamic properties of disordered zeolites of the natrolite group. Physics and Chemistry of Minerals, 29(4), 300-306.

Paukov, I.E., Belitskii, I.A., and Kovalevskaya, Y.A. (2002c) Thermodynamic properties of the natural zeolite harmotome at low temperatures. Geokhimiya(5), 568-571.

Qiu, L., Laws, P.A., Zhan, B.-Z., and White, M.A. (2006) Thermodynamic investigations of zeolites NaX and NaY. Canadian journal of chemistry, 84(2), 134-139.

Qiu, L., Murashov, V., and White, M.A. (2000) Zeolite 4A: heat capacity and thermodynamic properties. Solid state sciences, 2(8), 841-846.

Rosen, P.F., Dickson, M.S., Calvin, J.J., Ross, N.L., Friščić, T., Navrotsky, A., and Woodfield, B.F. (2020) Thermodynamic Evidence of Structural Transformations in CO2-Loaded Metal–Organic Framework Zn (MeIm) 2 from Heat Capacity Measurements. Journal of the American Chemical Society, 142(10), 4833-4841.

Schliesser, J.M., and Woodfield, B.F. (2015a) Development of a Debye heat capacity model for vibrational modes with a gap in the density of states. Journal of Physics: Condensed Matter, 27(28), 285402.

-. (2015b) Lattice vacancies responsible for the linear dependence of the low-temperature heat capacity of insulating materials. Physical Review B, 91(2), 024109.

Shi, Q., Boerio-Goates, J., and Woodfield, B.F. (2011) An improved technique for accurate heat capacity measurements on powdered samples using a commercial relaxation calorimeter. The Journal of Chemical Thermodynamics, 43(8), 1263-1269.

Smith, S.J., Lang, B.E., Liu, S., Boerio-Goates, J., and Woodfield, B.F. (2007) Heat capacities and thermodynamic functions of hexagonal ice from T= 0.5 K to T= 38 K. The Journal of Chemical Thermodynamics, 39(5), 712-716.

Sugisaki, M., Suga, H., and Seki, S. (1968) Calorimetric study of the glassy state. IV. Heat capacities of glassy water and cubic ice. Bulletin of the Chemical Society of Japan, 41(11), 2591-2599.

Sun, H., Wu, D., Liu, K., Guo, X., and Navrotsky, A. (2016) Energetics of alkali and alkaline earth ion-exchanged zeolite A. The Journal of Physical Chemistry C, 120(28), 15251-15256.

Vieillard, P. (2010) A predictive model for the entropies and heat capacities of zeolites. European Journal of Mineralogy, 22(6), 823-836.

Voskov, A.L., Voronin, G.F., Kutsenok, I.B., and Kozin, N.Y. (2019) Thermodynamic database of zeolites and new method of their thermodynamic properties evaluation for a wide temperature range. Calphad, 66, 101623.

Wu, L., and Navrotsky, A. (2016) Synthesis and thermodynamic study of transition metal ion (Mn 2+, Co 2+, Cu 2+, and Zn 2+) exchanged zeolites A and Y. Physical Chemistry Chemical Physics, 18(15), 10116-10122.

Yang, S., and Navrotsky, A. (2000) Energetics of formation and hydration of ion-exchanged zeolite Y. Microporous and Mesoporous Materials, 37(1-2), 175-186.

Yin, X., Zhu, G., Yang, W., Li, Y., Zhu, G., Xu, R., Sun, J., Qiu, S., and Xu, R. (2005) Stainless - Steel - Net - Supported Zeolite NaA Membrane with High Permeance and High Permselectivity of Oxygen over Nitrogen. Advanced Materials, 17(16), 2006-2010.

This is the peer-reviewed, final accepted version for American Mineralogist, published by the Mineralogical Society of America.
The published version is subject to change. Cite as Authors (Year) Title. American Mineralogist, in press.
DOI: https://doi.org/10.2138/am-2021-7726. http://www.minsocam.org/

Table 1. Chemical formulas for zeolites with low-temperature heat capacity measurements in the literature. Formulas have been normalized to the form (Cations)$Al_xSi_yO_2$.

Zeolite Name	Chemical Formula	mol H_2O	mol extra-framework cations	Si/Al ratio	Ref.
Gmelinite	$(Na_{0.232}K_{0.002}Ca_{0.035}Fe_{0.002})Al_{0.305}Si_{0.695}O_2$	0.978	0.270	2.3	(Paukov et al., 2001a)
Tl Natrolite	$(Tl_{0.374}Na_{0.01}Mg_{0.006})Al_{0.396}Si_{0.604}O_2$	0.466	0.39	1.5	(Paukov et al., 2005)
‡ Laumontite 1	$(Ca_{0.17})Al_{0.33}Si_{0.67}O_2$	0.722	0.17	2.0	(Paukov and Fursenko, 1998a)
‡ Laumontite 2 (Leonhardite)	$(Ca_{0.17})Al_{0.33}Si_{0.67}O_2$	0.615	0.17	2.0	(Paukov and Fursenko, 1998b)
‡ Paranatrolite	$(Na_{0.380}K_{0.044}Ca_{0.01})Al_{0.448}Si_{0.552}O_2$	0.620	0.436	1.2	(Paukov et al., 2002b)
‡ Tetranatrolite	$(Na_{0.380}K_{0.044}Ca_{0.01})Al_{0.448}Si_{0.552}O_2$	0.462	0.436	1.2	(Paukov et al., 2002b)
Thompsonite	$(Ca_{0.208}Na_{0.08})Al_{0.496}Si_{0.504}O_2$	0.63	0.29	5.4	(Paukov and Belitskii, 2000b)
Primary Leonhardite	$(Na_{0.055}K_{0.072}Ca_{0.10})Al_{0.330}Si_{0.670}O_2$	0.545	0.228	2.0	(Paukov et al., 2002a)
Scolecite	$(Ca_{0.200}Na_{0.0005})Al_{0.4002}Si_{0.5995}O_2$	0.6010	0.2005	1.5	(Johnson et al., 1983)
‡† Na Zeolite A	$(Na_{0.5})Al_{0.5}Si_{0.5}O_2$	0	0.5	1.0	(Qiu et al., 2000)
Bikitaite	$(Li_{0.35})Al_{0.333}Si_{0.662}O_2$	0.318	0.35	2.0	(Paukov et al., 1998b)
‡ Analcime	$(Na_{0.32})Al_{0.32}Si_{0.68}O_2$	0.33	0.32	2.1	(Johnson et al., 1982)
‡ Analcime dehydrated	$(Na_{0.32})Al_{0.32}Si_{0.68}O_2$	0	0.32	2.1	(Johnson et al., 1982)
‡ Mordenite	$(Ca_{0.0482}Na_{0.0602})Al_{0.157}Si_{0.843}O_2$	0.5780	0.1084	5.4	(Johnson et al., 1992)
‡ Mordenite dehydrated	$(Ca_{0.0482}Na_{0.0602})Al_{0.157}Si_{0.843}O_2$	0	0.1084	5.4	(Johnson et al., 1992)
* Brewsterite	$(Sr_{0.081}Ba_{0.041}Na_{0.004}K_{0.001})Al_{0.250}Si_{0.750}O_2$	0.631	0.128	3.0	(Paukov et al., 2001b)
* Chabazite	$(Ca_{0.138}Na_{0.020}K_{0.008})Al_{0.316}Si_{0.688}O_2$	1.04	0.166	2.1	(Drebushchak, 1990)
* Clinoptilolite 1	$(Sr_{0.0020}Mg_{0.00689}Ca_{0.0423}Mn_{0.0001}Ba_{0.0034}K_{0.0302}Na_{0.053})Al_{0.192}Fe_{0.00094}Si_{0.80739}O_2$	0.60678	0.138	4.2	(Johnson et al., 1991)
* Clinoptilolite 2	$(Na_{0.016}K_{0.027}Ca_{0.0417}Mg_{0.0342})Al_{0.19}Fe_{0.008}Si_{0.81}O_2$	0.61	0.119	4.3	(Hemingway and Robie, 1984)
* Epistilbite	$(Ca_{0.10}Na_{0.042}K_{0.0075})Al_{0.25}Si_{0.75}O_2$	0.638	0.15	3.0	(Paukov et al., 1998a)
* Erionite	$(Mg_{0.032}Ca_{0.057}Na_{0.013}K_{0.066})Al_{0.237}Si_{0.758}O_2$	0.802	0.168	3.2	(Paukov et al., 1998c)
* Ferrierite	$(Ca_{0.033}Mg_{0.01}Na_{0.070}K_{0.008})Al_{0.170}Fe_{0.002}Si_{0.828}O_2$	0.482	0.12	4.9	(Paukov and Belitskii, 2000a)
* Harmotome	$(Ba_{0.12}Ca_{0.006}Na_{0.029}K_{0.01})Al_{0.298}Si_{0.702}O_2$	0.742	0.17	2.4	(Paukov et al., 2002c)
* Heulandite 1	$(Ba_{0.0072}Sr_{0.0194}Ca_{0.0650}K_{0.0147}Na_{0.0426})Al_{0.2406}Si_{0.7594}O_2$	0.667	0.15	3.2	(Johnson et al., 1985)
* Heulandite 2	$(Na_{0.0406}K_{0.066}Ca_{0.0957})Al_{0.2376}Si_{0.762}O_2$	0.686	0.202	3.2	(Drebushchak, 1990)
*† Merlinoite P-9(NaK)	$(Na_{0.28}K_{0.065})Al_{0.34}Si_{0.660}O_2$	0.724	0.34	1.9	(Donahoe et al., 1990)
*† Merlinoite P-9(KNa)	$(K_{0.27}Na_{0.068})Al_{0.34}Si_{0.660}O_2$	0.616	0.34	1.9	(Donahoe et al., 1990)
*† Merlinoite P-9(K)	$(K_{0.34})Al_{0.34}Si_{0.660}O_2$	0.575	0.34	1.9	(Donahoe et al., 1990)
*† Merlinoite P-8(NaK)	$(Na_{0.29}K_{0.068})Al_{0.36}Si_{0.644}O_2$	0.776	0.36	1.8	(Donahoe et al., 1990)
*† Merlinoite P-8(KNa)	$(K_{0.32}Na_{0.03})Al_{0.36}Si_{0.573}O_2$	0.637	0.36	1.8	(Donahoe et al., 1990)
*† Merlinoite P-8(K)	$(K_{0.36})Al_{0.36}Si_{0.644}O_2$	0.601	0.36	1.8	(Donahoe et al., 1990)
* Phillipsite	$(Na_{0.135}K_{0.1})Al_{0.235}Si_{0.765}O_2$	0.8	0.2	3.3	(Hemingway and Robie, 1984)
* Stellerite	$(Ca_{0.118})Al_{0.228}Si_{0.770}O_2$	0.787	0.118	3.4	(Paukov et al., 1997)
* Stilbite	$(Ca_{0.1132}Na_{0.0151}K_{0.0007})Al_{0.2422}Si_{0.7578}O_2$	0.814	0.1290	3.1	(Howell et al., 1990)

*Not pictured in Figure 1; heat capacity lies within the grey region bounded by gmelinite and scolecite.
†Synthetic zeolite.
‡Used to calculate zeolitic water heat capacity for Figure 3.

Table 2. Sample compositions, water content, and color of samples. (Na is not listed with a coefficient <0.01.)

	Sample Composition	Exchange level (%)	Color before Dehydration	Color after dehydration
Na-A	$Na_{0.480}Al_{0.491}Si_{0.509}O_2{\cdot}0.23\ H_2O$	N/A	White	White
Zn-A	$Zn_{0.24}Al_{0.52}Si_{0.49}O_2{\cdot}0.58\ H_2O$	99.2	White	White

DOI: https://doi.org/10.2138/am-2021-7726. http://www.minsocam.org/

Table 3. Details of the PPMS calorimetric measurements including pressures (p), sample mass (M_s), sample molar mass (M), and copper mass (M_{Cu}). The estimated standard uncertainties in the masses $M_{s,Cu}$ and pressure p are $u(M_{s,Cu})$ = 0.06 mg and $u(p)$ = 0.1 mPa.

	Na-A·0.23 H_2O	Zn-A·0.58 H_2O
p / mPa	1.2	1.2
M_s / mg	9.86	8.76
M / g·mol^{-1}	74.5992	86.00
M_{Cu} / mg	39.20	25.48

Table 4. Measured molar heat capacity values at constant pressure for Na-A·0.23 H_2O. M = 74.5992 g·mol^{-1}. Measurements were performed on a PPMS with a standard uncertainty of 2% $C_{p,m}$ below about T = 10 K and 1% $C_{p,m}$ from T = (10 to 300) K. The standard uncertainty in temperature is about 4 mK.

T/K	$C_{p,m}$/J·K^{-1}·mol^{-1}	T/K	$C_{p,m}$/J·K^{-1}·mol^{-1}	T/K	$C_{p,m}$/J·K^{-1}·mol^{-1}
1.8375	$1.9550 \cdot 10^{-3}$	7.9024	0.15485	77.367	22.369
1.9188	$2.2559 \cdot 10^{-3}$	8.2502	0.18222	84.507	25.039
1.9989	$2.6448 \cdot 10^{-3}$	8.6156	0.21000	92.366	27.569
2.0823	$3.0269 \cdot 10^{-3}$	8.9947	0.23067	100.95	29.959
2.1707	$3.3410 \cdot 10^{-3}$	9.3933	0.26904	111.05	33.032
2.2647	$3.5862 \cdot 10^{-3}$	9.8059	0.30471	121.12	36.069
2.3625	$4.1142 \cdot 10^{-3}$	10.254	0.35263	131.24	38.802
2.4638	$4.4779 \cdot 10^{-3}$	10.716	0.40102	141.32	41.575
2.5689	$4.9190 \cdot 10^{-3}$	11.193	0.45588	151.39	44.341
2.6788	$4.8905 \cdot 10^{-3}$	11.688	0.51531	161.51	46.952
2.8005	$5.7169 \cdot 10^{-3}$	12.204	0.58382	171.62	49.474
2.9217	$6.6170 \cdot 10^{-3}$	12.743	0.66150	181.70	52.243
3.0503	$7.1500 \cdot 10^{-3}$	13.308	0.74529	191.79	54.671
3.1846	$8.3924 \cdot 10^{-3}$	13.894	0.83895	201.89	57.016
3.3266	0.010003	14.510	0.94536	211.99	59.326
3.4734	0.011705	15.152	1.0586	222.09	61.565
3.6269	0.012551	15.661	1.1561	232.18	63.565
3.7867	0.014456	17.110	1.4553	242.26	65.747
3.9545	0.015006	18.698	1.8199	252.35	67.944
4.1297	0.019355	20.426	2.2436	262.46	69.826
4.3143	0.022040	22.331	2.7595	272.57	71.364
4.5075	0.025865	24.403	3.3592	282.66	72.916
4.7042	0.026889	26.663	4.0671	292.76	74.413
4.9124	0.034383	29.139	4.8734	302.86	76.330
5.1269	0.037835	31.848	5.8112		
5.3524	0.041819	34.804	6.8650		
5.5907	0.047313	38.039	8.0291		
5.8366	0.057173	41.573	9.3510		
6.0954	0.070791	45.430	10.841		
6.3678	0.074954	49.649	12.298		
6.6459	0.090640	54.254	14.061		
6.9406	0.10316	59.282	15.900		
7.2475	0.11629	64.783	17.833		
7.5651	0.13378	70.797	19.884		

Table 5. Measured molar heat capacity values at constant pressure for Zn-A·0.58 H_2O. M = 86.00 g·mol^{-1}. Measurements were performed on a PPMS with a standard uncertainty of 2% $C_{p,m}$ below about T = 10 K and 1% $C_{p,m}$ from T = (10 to 300) K. The standard uncertainty in temperature is about 4 mK.

T/K	$C_{p,m}$/J·K^{-1}·mol^{-1}	T/K	$C_{p,m}$/J·K^{-1}·mol^{-1}	T/K	$C_{p,m}$/J·K^{-1}·mol^{-1}
1.8347	$2.2992 \cdot 10^{-3}$	7.8851	0.10498	77.366	18.694
1.9052	$2.5956 \cdot 10^{-3}$	8.2360	0.11373	84.517	21.259
1.9875	$2.9279 \cdot 10^{-3}$	8.6000	0.14273	92.375	23.763
2.0731	$2.9471 \cdot 10^{-3}$	8.9813	0.14990	100.95	25.956
2.1650	$3.2954 \cdot 10^{-3}$	9.3793	0.16506	111.05	28.831
2.2603	$3.8977 \cdot 10^{-3}$	9.7932	0.19097	121.10	31.742
2.3595	$4.1933 \cdot 10^{-3}$	10.249	0.22503	131.22	34.451
2.4623	$4.6734 \cdot 10^{-3}$	10.706	0.25338	141.30	37.014
2.5695	$5.0394 \cdot 10^{-3}$	11.179	0.28566	151.36	39.595
2.6791	$4.8942 \cdot 10^{-3}$	11.673	0.32357	161.47	42.029
2.7952	$6.2735 \cdot 10^{-3}$	12.189	0.36689	171.57	44.432
2.9187	$6.6484 \cdot 10^{-3}$	12.730	0.41716	181.65	46.665
3.0457	$7.4692 \cdot 10^{-3}$	13.296	0.47392	191.73	48.959
3.1797	$7.8765 \cdot 10^{-3}$	13.886	0.53748	201.83	51.183
3.3231	$8.6734 \cdot 10^{-3}$	14.503	0.60884	211.92	53.094
3.4688	0.010991	15.142	0.68617	222.02	55.170
3.6167	0.010808	15.651	0.75333	232.10	56.918
3.7753	0.013065	17.100	0.96206	242.18	58.928
3.9434	0.014829	18.684	1.2198	252.27	60.886
4.1175	0.015476	20.407	1.5310	262.37	62.326
4.3015	0.018158	22.320	1.9043	272.48	64.236
4.4898	0.019505	24.392	2.3574	282.57	65.593
4.6864	0.022401	26.653	2.8978	292.66	67.317
4.8934	0.028756	29.124	3.5343	302.75	69.189
5.1098	0.032146	31.830	4.2699		
5.3370	0.032338	34.787	5.1342		
5.5724	0.037815	38.023	6.0854		
5.8192	0.045025	41.564	7.1685		
6.0794	0.044861	45.420	8.4470		
6.3508	0.054527	49.638	9.7004		
6.6296	0.063879	54.241	11.198		
6.9236	0.074276	59.271	12.846		
7.2305	0.079946	64.776	14.608		
7.5520	0.090133	70.789	16.474		

DOI: https://doi.org/10.2138/am-2021-7726. http://www.minsocam.org/

Table 6. Parameters for low T (< 15 K), mid T (5 K < T < 60 K), and high T (T > 50 K) fits of heat capacity data (in $J \cdot K^{-1} \cdot mol^{-1}$) for Na-A·0.23 H_2O and Zn-A·0.58 H_2O.

	Parameter	Na-A·0.23 H_2O	Zn-A·0.58 H_2O
Low T Fits	γ / $J \cdot K^{-2} \cdot mol^{-1}$	$4.8689 \cdot 10^{-4}$	$8.5878 \cdot 10^{-4}$
	B_3 / $J \cdot K^{-4} \cdot mol^{-1}$	$2.0795 \cdot 10^{-4}$	$1.3218 \cdot 10^{-4}$
	B_5 / $J \cdot K^{-6} \cdot mol^{-1}$	$1.0964 \cdot 10^{-8}$	$3.0090 \cdot 10^{-7}$
	B_7 / $J \cdot K^{-8} \cdot mol^{-1}$	$-2.7525 \cdot 10^{-10}$	$-6.5592 \cdot 10^{-10}$
	B_{gap}	0.10669	$1.3734 \cdot 10^{-2}$
	n	1	1
	δ	22.342	11.863
	%RMS	3.78	1.14
	Range / K	1.83–11.53	1.83–8.24
Mid T Fits	A_0 / $J \cdot K^{-1} \cdot mol^{-1}$	$-9.5956 \cdot 10^{-2}$	0.10738
	A_1 / $J \cdot K^{-2} \cdot mol^{-1}$	$6.5577 \cdot 10^{-2}$	$-5.6575 \cdot 10^{-2}$
	A_2 / $J \cdot K^{-3} \cdot mol^{-1}$	$-1.6117 \cdot 10^{-2}$	$1.2212 \cdot 10^{-2}$
	A_3 / $J \cdot K^{-4} \cdot mol^{-1}$	$2.1934 \cdot 10^{-3}$	$-1.1865 \cdot 10^{-3}$
	A_4 / $J \cdot K^{-5} \cdot mol^{-1}$	$-1.0653 \cdot 10^{-4}$	$9.2839 \cdot 10^{-5}$
	A_5 / $J \cdot K^{-6} \cdot mol^{-1}$	$2.9553 \cdot 10^{-6}$	$-3.6479 \cdot 10^{-6}$
	A_6 / $J \cdot K^{-7} \cdot mol^{-1}$	$-4.8570 \cdot 10^{-8}$	$7.5423 \cdot 10^{-8}$
	A_7 / $J \cdot K^{-8} \cdot mol^{-1}$	$4.3582 \cdot 10^{-10}$	$-7.9096 \cdot 10^{-10}$
	A_8 / $J \cdot K^{-9} \cdot mol^{-1}$	$-1.6364 \cdot 10^{-12}$	$3.3174 \cdot 10^{-12}$
	%RMS	0.16	2.48
	Range / K	11.53–49.22	8.24–55.375
High T Fits	m / mol	0.70826	0.91488
	Θ_D / K	166.22	230.57
	n_1 / mol	1.3526	1.3657
	Θ_{E1} / K	341.50	448.06
	n_2 / mol	2.2769	1.8853
	Θ_{E2} / K	904.36	1069.7
	%RMS	0.32	0.48
	Range / K	49.22–302.86	55.375–302.75

Table 7. Standard thermodynamic functions of partially dehydrated Na-A·0.23 H_2O. M = 74.5992 g·mol^{-1}. All calculated thermodynamic values have an estimated standard uncertainty of about 0.02 X below 10 K and 0.01 X above 10 K where X represents the thermodynamic property.

T/K	$C_{p,m}$/J·K^{-1}·mol^{-1}	$\Delta_0^T S_m^o$/J·K^{-1}·mol^{-1}	$\Delta_0^T H_m^o$/kJ·mol^{-1}	Φ_m^o/J·K^{-1}·mol^{-1}
0	0	0	0	0
1	$6.948\cdot10^{-4}$	$5.562\cdot10^{-4}$	$2.954\cdot10^{-7}$	$2.608\cdot10^{-4}$
2	$2.641\cdot10^{-3}$	$1.529\cdot10^{-3}$	$1.806\cdot10^{-6}$	$6.255\cdot10^{-4}$
3	$7.264\cdot10^{-3}$	$3.353\cdot10^{-3}$	$6.458\cdot10^{-6}$	$1.200\cdot10^{-3}$
4	0.01686	$6.603\cdot10^{-3}$	$1.798\cdot10^{-5}$	$2.107\cdot10^{-3}$
5	0.03456	0.01209	$4.289\cdot10^{-5}$	$3.510\cdot10^{-3}$
6	0.06330	0.02074	$9.079\cdot10^{-5}$	$5.610\cdot10^{-3}$
7	0.10539	0.03348	$1.739\cdot10^{-4}$	$8.628\cdot10^{-3}$
8	0.16243	0.05110	$3.066\cdot10^{-4}$	0.01278
9	0.23553	0.07429	$5.042\cdot10^{-4}$	0.01827
10	0.32541	0.10361	$7.832\cdot10^{-4}$	0.02529
15	1.0324	0.35481	$3.999\cdot10^{-3}$	0.08821
20	2.1363	0.79456	0.01177	0.20586
25	3.5435	1.4177	0.02587	0.38300
30	5.1663	2.2045	0.04757	0.61890
35	6.9322	3.1321	0.07777	0.91012
40	8.7739	4.1775	0.11702	1.2521
45	10.632	5.3182	0.16553	1.6397
50	12.467	6.5339	0.22331	2.0678
60	16.101	9.1265	0.36606	3.0256
70	19.765	11.884	0.54543	4.0925
80	23.314	14.757	0.76096	5.2451
90	26.670	17.699	1.0111	6.4649
100	29.827	20.674	1.2937	7.7369
110	32.820	23.658	1.6070	9.0486
120	35.693	26.638	1.9497	10.390
130	38.485	29.605	2.3206	11.754
140	41.219	32.558	2.7192	13.135
150	43.909	35.494	3.1449	14.528
160	46.556	38.412	3.5972	15.929
170	49.155	41.313	4.0758	17.337
180	51.699	44.195	4.5802	18.749
190	54.178	47.057	5.1096	20.164
200	56.584	49.897	5.6635	21.580
210	58.908	52.715	6.2410	22.995
220	61.146	55.507	6.8414	24.410
230	63.292	58.273	7.4636	25.822
240	65.345	61.010	8.1069	27.231
250	67.303	63.718	8.7702	28.637
260	69.167	66.394	9.4526	30.038
270	70.939	69.038	10.153	31.433
273.15	71.478	69.864	10.378	31.872
280	72.621	71.648	10.871	32.823
290	74.215	74.225	11.605	34.206
298.15	75.451	76.299	12.215	35.329
300	75.725	76.766	12.355	35.583

DOI: https://doi.org/10.2138/am-2021-7726. http://www.minsocam.org/

Table 8. Standard thermodynamic functions of partially dehydrated Zn-A·0.58 H_2O. M = 86.00 $g \cdot mol^{-1}$. All calculated thermodynamic values have an estimated standard uncertainty of about 0.02 X below 10 K and 0.01 X above 10 K where X represents the thermodynamic property.

T/K	$C_{p,m}$/J·K^{-1}·mol^{-1}	$\Delta_0^T S_m^\circ$/J·K^{-1}·mol^{-1}	$\Delta_0^T H_m^\circ$/kJ·mol^{-1}	Φ_m°/J·K^{-1}·mol^{-1}
0	0	0	0	0
1	$9.914 \cdot 10^{-4}$	$9.029 \cdot 10^{-4}$	$4.625 \cdot 10^{-7}$	$4.404 \cdot 10^{-4}$
2	$2.857 \cdot 10^{-3}$	$2.081 \cdot 10^{-3}$	$2.266 \cdot 10^{-6}$	$9.482 \cdot 10^{-4}$
3	$7.007 \cdot 10^{-3}$	$3.919 \cdot 10^{-3}$	$6.937 \cdot 10^{-6}$	$1.607 \cdot 10^{-3}$
4	0.01502	$6.925 \cdot 10^{-3}$	$1.757 \cdot 10^{-5}$	$2.531 \cdot 10^{-3}$
5	0.02811	0.01158	$3.867 \cdot 10^{-5}$	$3.844 \cdot 10^{-3}$
6	0.04727	0.01830	$7.581 \cdot 10^{-5}$	$5.662 \cdot 10^{-3}$
7	0.07352	0.02746	$1.356 \cdot 10^{-4}$	$8.090 \cdot 10^{-3}$
8	0.10797	0.03943	$2.256 \cdot 10^{-4}$	0.01123
9	0.15254	0.05461	$3.549 \cdot 10^{-4}$	0.01517
10	0.20774	0.07344	$5.342 \cdot 10^{-4}$	0.02003
15	0.66428	0.23331	$2.582 \cdot 10^{-3}$	0.06120
20	1.4492	0.52416	$7.730 \cdot 10^{-3}$	0.13764
25	2.5201	0.95810	0.01755	0.25597
30	3.7831	1.5270	0.03325	0.41864
35	5.1671	2.2128	0.05558	0.62468
40	6.6558	2.9987	0.08509	0.87134
45	8.2535	3.8739	0.12233	1.1555
50	9.9123	4.8293	0.16774	1.4745
60	13.109	6.9190	0.28283	2.2050
70	16.342	9.1825	0.43009	3.0384
80	19.563	11.575	0.60964	3.9548
90	22.727	14.063	0.82116	4.9390
100	25.788	16.617	1.0638	5.9786
110	28.721	19.214	1.3365	7.0635
120	31.522	21.834	1.6378	8.1851
130	34.200	24.463	1.9665	9.3361
140	36.772	27.092	2.3215	10.511
150	39.253	29.715	2.7017	11.703
160	41.656	32.325	3.1063	12.911
170	43.990	34.921	3.5345	14.129
180	46.261	37.500	3.9859	15.356
190	48.470	40.060	4.4596	16.589
200	50.619	42.601	4.9551	17.826
210	52.705	45.122	5.4717	19.066
220	54.727	47.621	6.0090	20.307
230	56.684	50.097	6.5661	21.549
240	58.572	52.549	7.1424	22.789
250	60.391	54.977	7.7373	24.028
260	62.141	57.380	8.3500	25.265
270	63.821	59.757	8.9799	26.499
273.15	64.335	60.501	9.1817	26.886
280	65.431	62.108	9.6262	27.728
290	66.972	64.431	10.288	28.954
298.15	68.179	66.304	10.839	29.949
300	68.446	66.726	10.965	30.175

DOI: https://doi.org/10.2138/am-2021-7726. http://www.minsocam.org/

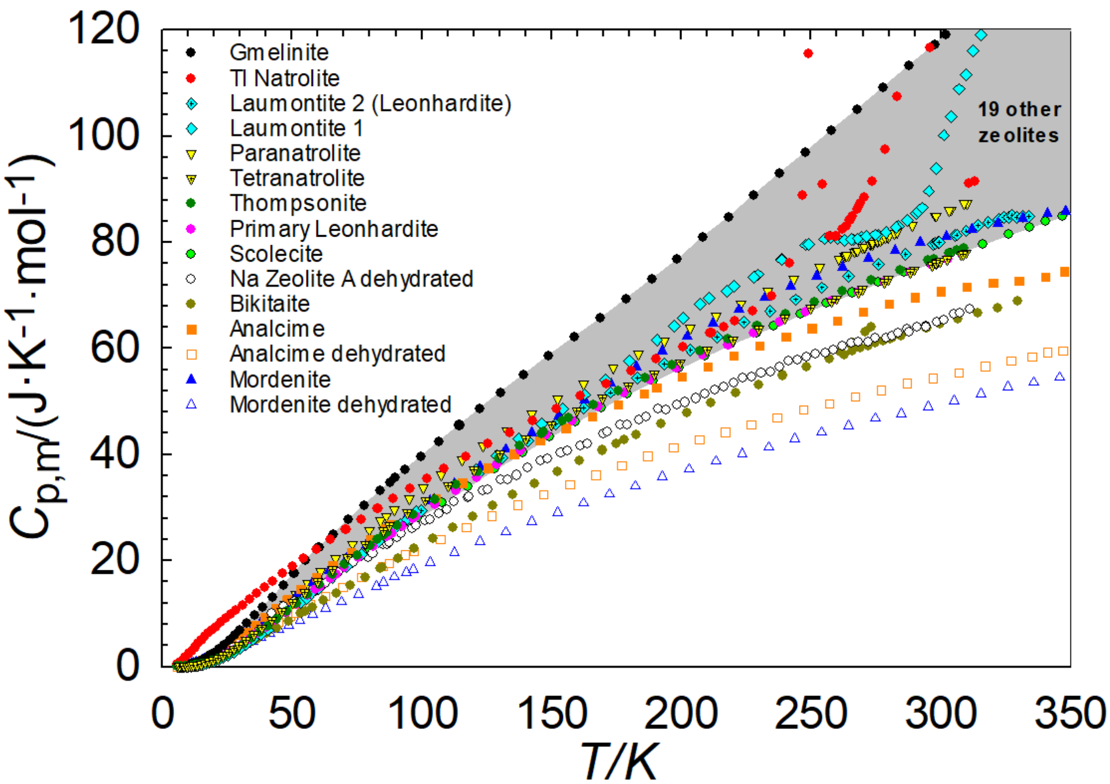

Figure 1. Low-temperature zeolite heat capacities from the literature, with formulas standardized to the form (Cations)$Al_xSi_yO_2$. 19 densely spaced data sets were excluded; their heat capacity curves fall within the shaded region bounded by gmelinite and scolecite. Three high data points for Tl natrolite were also excluded.

This is the peer-reviewed, final accepted version for American Mineralogist, published by the Mineralogical Society of America.
The published version is subject to change. Cite as Authors (Year) Title. American Mineralogist, in press.
DOI: https://doi.org/10.2138/am-2021-7726. http://www.minsocam.org/

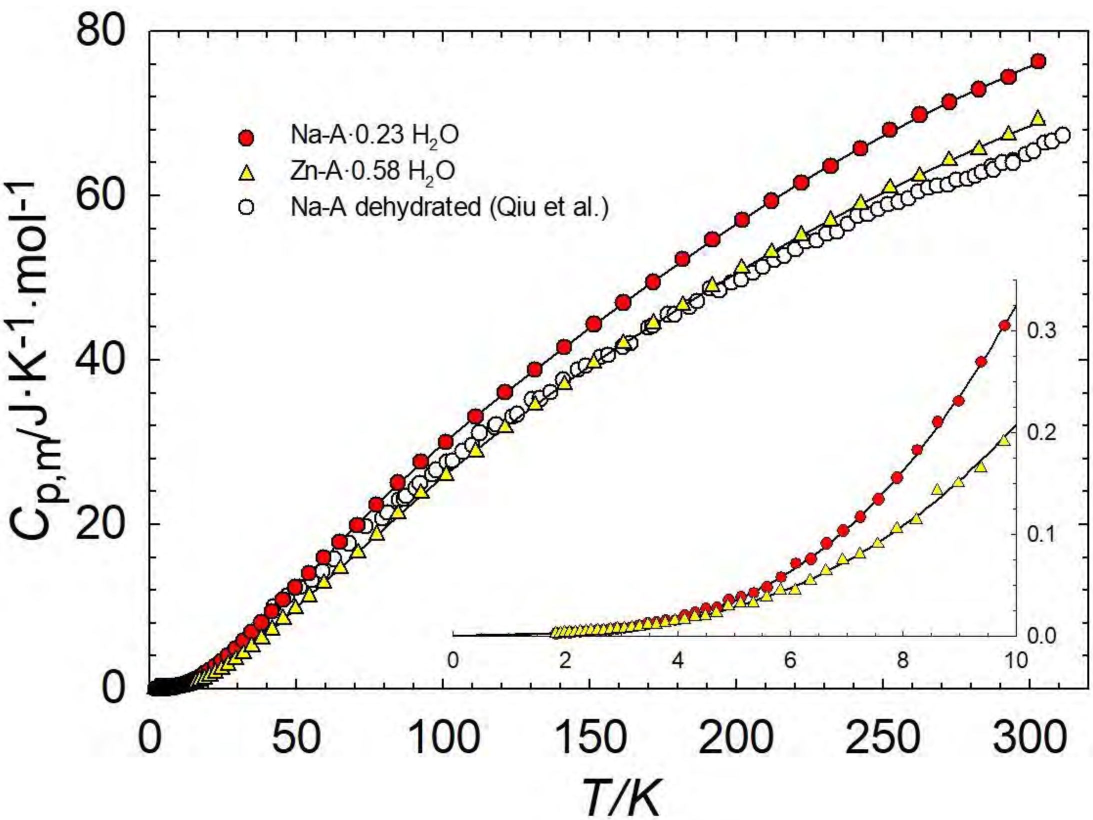

Figure 2. Heat capacity as a function of temperature for Na-A·0.23 H_2O and Zn-A·0.58 H_2O, with literature data (Qiu et al., 2000) for fully dehydrated Na-A. Fits are provided behind the data points. Inset shows data below 10 K. Literature data are not included in the low-T inset because they do not extend below 37 K.

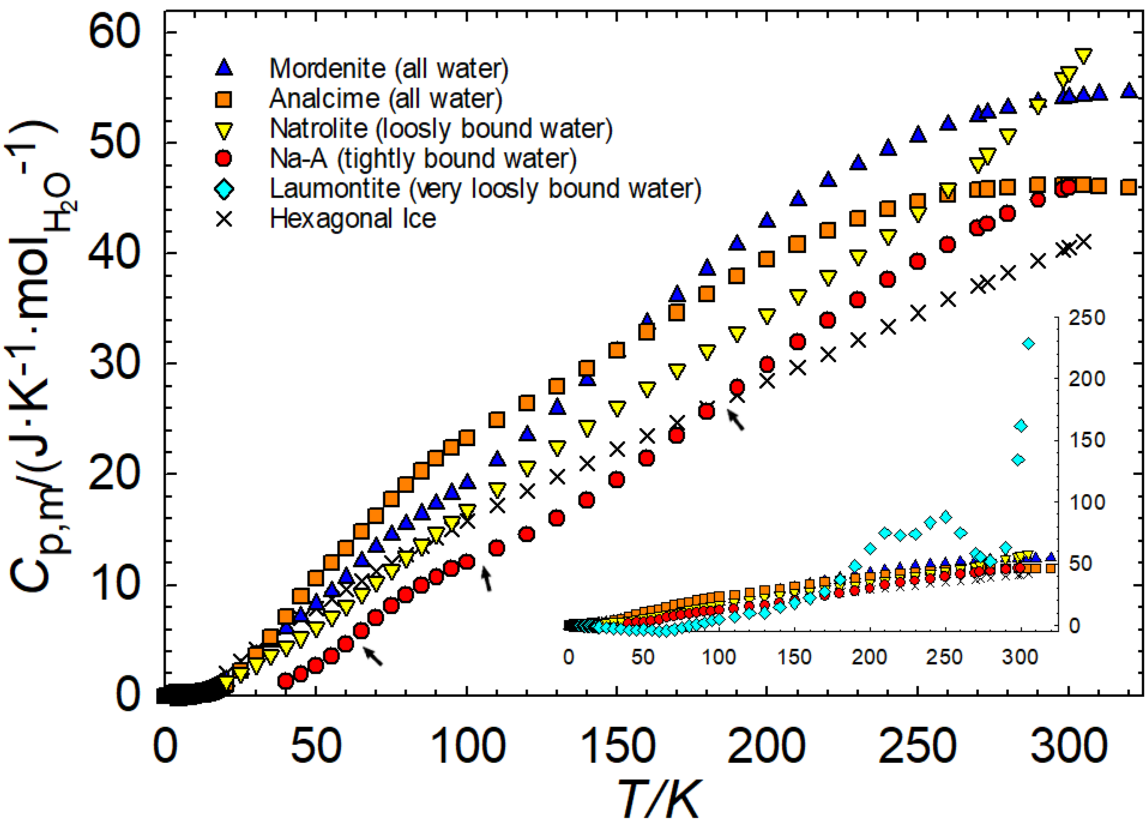

Figure 3. Heat capacity of zeolitic water in zeolites Na-A, mordenite (Johnson et al., 1992), analcime (Johnson et al., 1982), natrolite (Paukov et al., 2002b), and laumontite (Paukov and Fursenko, 1998a; Paukov and Fursenko, 1998b) with literature data for hexagonal ice (Flubacher et al., 1960; Giauque and Stout, 1936; Haida et al., 1974; Handa and Klug, 1988; Smith et al., 2007; Sugisaki et al., 1968). Arrows highlight inflection points in the data set representing water in Na-A. Inset shows the data with different scaling for comparison with zeolitic water in laumontite.